

Geophysical Research Letters

RESEARCH LETTER

10.1029/2019GL084961

Key Points:

- Seismic anisotropy may be explained by a rollback of the Indian slab and modulation by a slab gap
- The rotational pattern of fast orientations in SE Tibetan Plateau may be attributed to flow in the mantle wedge escaped from the slab gap
- N-S anisotropy in NE India and Burma block and E-W anisotropy in Indochina may reflect sub-slab trench parallel flow from slab rollback

Supporting Information:

- Supporting Information S1

Correspondence to:

L. Liu, and S. S. Gao,
lltrc@mst.edu
sgao@mst.edu

Citation:

Liu, L., Gao, S. S., Liu, K. H., Li, S., Tong, S., & Kong, F. (2019). Toroidal mantle flow induced by slab subduction and rollback beneath the Eastern Himalayan syntaxis and adjacent areas. *Geophysical Research Letters*, *46*, 11,080–11,090. <https://doi.org/10.1029/2019GL084961>

Received 12 AUG 2019

Accepted 16 SEP 2019

Published online 28 OCT 2019

Toroidal Mantle Flow Induced by Slab Subduction and Rollback Beneath the Eastern Himalayan Syntaxis and Adjacent Areas

Lin Liu^{1,2,3} , Stephen S. Gao² , Kelly H. Liu² , Sanzhong Li¹, Siyou Tong¹, and Fansheng Kong⁴ 

¹Key Laboratory of Submarine Geosciences and Prospecting Techniques, Ministry of Education, College of Marine Geosciences, Ocean University of China, Qingdao, China, ²Geology and Geophysics Program, Missouri University of Science and Technology, Rolla, MO, USA, ³Department of Geophysics, Stanford University, Stanford, CA, USA, ⁴Key Laboratory of Submarine Geosciences, State Oceanic Administration, Second Institute of Oceanography, Ministry of Natural Resources, Hangzhou, China

Abstract A total of 431 well-defined and 632 null shear-wave splitting measurements obtained from 115 broadband seismic stations located in the eastern Himalayan syntaxis and adjacent areas is largely inconsistent with predicted fast orientations by absolute plate motion models. Spatial coherency analysis of the splitting parameters suggests that the observed azimuthal anisotropy is mostly located in the upper asthenosphere or the transitional layer between the lithosphere and asthenosphere, and the disagreement between the fast orientations and regional tectonic fabrics suggests an insignificant lithospheric contribution to the observed anisotropy. The observations may be attributed to flow systems that are driven by the westward rollback of the Indian slab beneath the Indo-Burma block and are modulated by a previously revealed gap between the northward and eastward subducting slabs of the Indian plate.

1. Introduction

The eastern Himalayan syntaxis (EHS), situated at the junction of the Indian plate, the Tibetan Plateau, and the Burma block (Figure 1), is characterized by two different styles of structural patterns (Bracciali et al., 2016; Zhang et al., 2004). One is a ductile contractional deformation system caused by the nearly N-S frontal Indian-Eurasian collision since ~50 Ma, and the other is lateral slip along the boundary, probably created by the subsequent indentation of the Indian plate into the Eurasian plate (Li et al., 2008; Yin & Harrison, 2000; Zhang et al., 2004). Approximately 20 mm/year of dextral motion is induced by the oblique subduction of the Indian plate beneath the Burma block along the Arakan trench since the middle to late Eocene (Argus et al., 2011; Ni et al., 1989; Powell & Conaghan, 1973; Steckler et al., 2016; Tapponnier et al., 1982). The northward subducting Indian slab is imaged by seismic tomographic investigations as a subhorizontal slab, located at a depth of about 100 km beneath the Himalayan Orogenic Belt and the Lhasa Terrane, and has reached the Bangong-Nujing Suture, which is the boundary between the Lhasa and Qiangtang Terranes (Figure 1; Li et al., 2013). For the eastward subduction, some tomographic images indicate that the slab has reached a depth of 300–400 km (Huang, Zhao, & Wang, 2015; Huang & Zhao, 2006; Li et al., 2008), while other studies (Huang, Wang, Xu, Wang, et al., 2015; Lei et al., 2009; Lei & Zhao, 2016) suggest that it has reached the mantle transition zone.

The existence of a slab gap beneath the EHS between the northward and eastward slabs has been suggested by some of the seismic tomographic studies (e.g., Giacomuzzi et al., 2012; Li et al., 2006; Lucente et al., 1999). The slab gap corresponds to a sudden break in seismicity (Dasgupta et al., 2003; Reyners et al., 1991) and negative velocity anomalies in the upper mantle (Li et al., 2006). Additionally, the presence of the gap is consistent with results of receiver function studies, which show depth variations of discontinuities in the crust and upper mantle (Kumar et al., 2016; Xu et al., 2018).

Geodynamic modeling and observational studies indicate that the dominant mantle flow field in active subduction zones is corner flow in the mantle wedge that is parallel to the downdip motion of the slab (Long & Silver, 2008, 2009). With appropriate trench migration velocity, trench-parallel and trench-perpendicular mantle flows may exist beneath and above the slab, respectively (Long & Becker, 2010; Long & Silver,

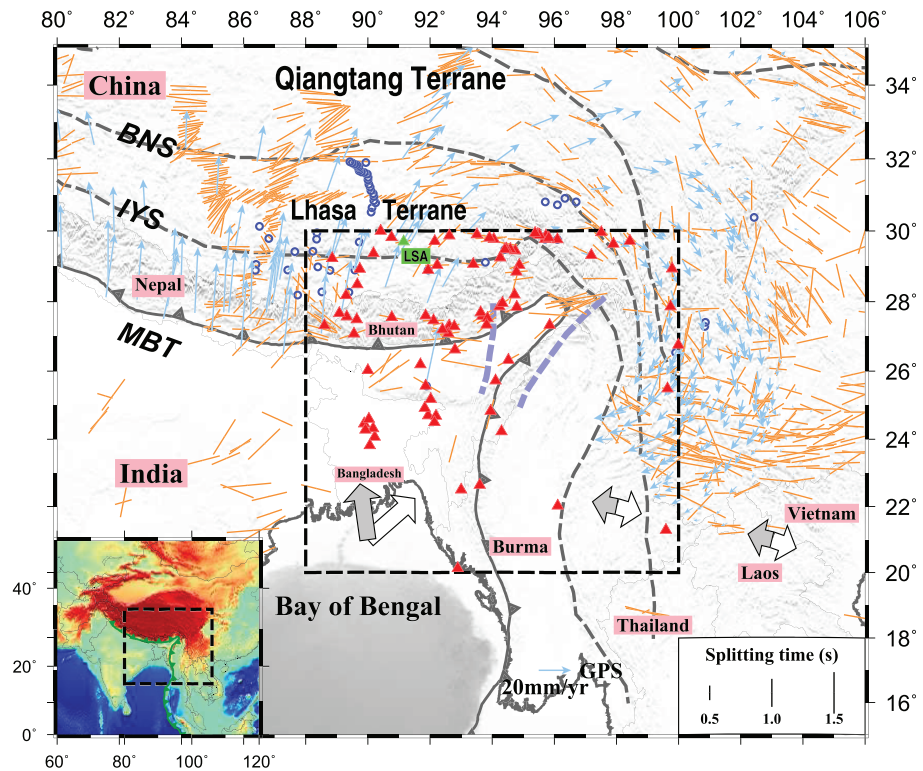


Figure 1. A topographic map of the southern and eastern Tibet and northern India showing major tectonic provinces (Hazarika et al., 2013). Orange bars represent measurements from more than 20 previous investigations (<http://splitting.gm.univ-montp2.fr/DB/public/searchdatabase.html>), while red triangles indicate stations used in this study. Station LSA is marked as a green triangle. Blue circles represent stations with all-null measurements from previous studies (Chen & Özalaybey, 1998; Flesch et al., 2005; Fu et al., 2008; Roy et al., 2012; Sol et al., 2007; Wang et al., 2008). Plate boundaries are from Socquet et al. (2006). White and gray arrows show the directions of the APM based on the NNR-MORVEL56 (Argus et al., 2011) and HS3-NUVEL1A models (Gripp & Gordon, 2002). The purple dash lines mark the gap between the northward and eastward subducting Indian slab segments indicated by Li et al. (2006). IYS: Indus-Yalu Suture; BNS: Bangong-Nujiang Suture; MBT: Main Boundary Thrust. Light blue arrows represent GPS velocity measurements relative to Eurasia (Gan et al., 2007). The mapped area of the main figure is outlined by the rectangle in the inset map, and our study area is outlined by the black dash lines in the main map.

2008). Previous modeling studies also suggest that an opening within a retreating slab may drive mantle material from the subslab region to the overlying mantle wedge, connecting the trench-parallel and trench-perpendicular return flow systems to a clockwise/anticlockwise toroidal flow around the slab edge (Becker & Faccenna, 2009; Duarte et al., 2013; Long & Wirth, 2013; Schellart, 2004; Stegman et al., 2006). However, direct observations for such a toroidal flow system are rare (Jadamec & Billen, 2010, 2012).

One of the most common constraints on the distribution of mantle flow systems is seismic azimuthal anisotropy as quantified by shear-wave splitting (SWS) analysis. As a commonly used tool to characterize mantle deformation, splitting of P-to-S converted waves at the core-mantle boundary (SKS, SKKS, and PKS, hereinafter referred to as XKS) has been used to provide insight into the deformation field in the lithosphere and asthenosphere in a wide range of tectonic settings (Long & Silver, 2009; Savage, 1999; Silver, 1996). Two XKS splitting parameters, the polarization orientation of the fast wave (fast orientation) and the arrival time difference between the fast and slow waves (splitting time), indicate the orientation and strength of seismic anisotropy accumulated along the ray path, respectively. While it is well-known that the XKS technique has a high lateral but low vertical resolution (Savage, 1999; Silver & Chan, 1991), under some circumstances, the optimal depth of anisotropy can be estimated using the spatial coherency of the splitting parameters (Gao & Liu, 2012).

Laboratory and observational investigations suggest that azimuthal anisotropy is dominantly caused by lattice preferred orientation (LPO) of anisotropic minerals in the upper mantle, principally olivine (Katayama &

Karato, 2006; Silver, 1996; Zhang & Karato, 1995). A number of mantle deformation processes have been proposed to explain the observed LPO. The first one is vertically coherent lithospheric deformation resulting from horizontal compression in which the resulting LPO is normal to the direction of maximum horizontal shortening. Another anisotropy-generating process is simple shear arising from the relative movement between the lithosphere and asthenosphere, which produces flow-parallel fast orientations in the lithosphere-asthenosphere transitional zone. The simple shear is commonly related to the absolute plate motion (APM) and other plate tectonic processes such as rifting, slab subduction, and slab rollback (Gao et al., 1994; Long & Becker, 2010; Schellart, 2004).

2. Previous SWS Studies in the Vicinity of the EHS

Most previous SWS investigations on seismic anisotropy presumably associated with the Indian-Eurasian convergence focus on the northward subduction zone (north of 26°N), where a clockwise rotation pattern of anisotropy is detected around the EHS (Figure 1; Chang et al., 2015; Hazarika et al., 2013; Sol et al., 2007; Wang et al., 2008). Most of the studies attribute the observed anisotropy to crust-mantle coupled deformation, on the basis of the consistency between the fast orientations from XKS splitting measurements and directions of surface deformation from global positioning system (GPS) measurements. One of the most puzzling observations is that in spite of the fact that the lithosphere beneath the Himalayan Orogenic Belt and the Lhasa Terrane has experienced considerable N-S compressional strain over the past tens of millions of years, weak or no azimuthal anisotropy is revealed by many SWS investigations in these areas (Chen et al., 2010; Fu et al., 2008; Huang et al., 2000; Zhao et al., 2014). To explain this, a two-layered model of anisotropy is proposed by Gao and Liu (2009) for station LSA, which is located in the northwestern portion of the study area (Figure 1). The top layer of anisotropy is related to lithospheric deformation, while the lower layer is probably caused by compressional stress or APM-induced mantle flow. This combined effect could explain the observed weak anisotropy, while accounting for ongoing deformation.

The SE Tibetan Plateau and the northern Indochina Peninsula show fast orientations that are parallel to the major strike slip faults (Figure 1). South of 26°N, there is a dramatic variation in the fast orientations, from N-S to E-W within less than 100 km (Figure 1; Flesch et al., 2005; Huang, Wang, Xu, Ding, et al., 2015; Kong et al., 2018; Lev et al., 2006; Sol et al., 2007; Wang et al., 2008). The fast orientations are significantly different from surface tectonic fabrics, conflicting with the hypothesis of lithospheric coherent deformation, and are likely related to mantle flow induced by the westward rollback of the subducted Indian plate beneath SE Tibet and Indochina (Kong et al., 2018; Yu et al., 2018).

On the Indian plate, while some early studies (Barruol & Hoffmann, 1999; Chen & Özalaybey, 1998; Sandvol et al., 1997) suggest a lack of observable splitting based on measurements at a few stations, significant anisotropy is detected by most of the more recent investigations (Figure 1; Hazarika et al., 2013; Heintz et al., 2009; Saikia et al., 2010, 2018; Singh et al., 2006, 2007). Using data from 56 broadband seismic stations in the eastern Himalayan and Burmese arc region, Saikia et al. (2018) report weak orogen-parallel anisotropy. Weak or the absence of anisotropy reported at stations on the Indian plate is attributed to multiple layers of anisotropy with nearly orthogonal fast orientations.

The present study is motivated by several factors. The first is a significant increase in the number of broadband seismic stations with available data in the previously sparsely sampled area (Figure 1). As demonstrated below, the greatly improved station coverage over previous studies is essential for the proposed mantle flow model associated with the two subduction systems and the slab gap between them. The second rationale for the current study is that most previous investigations only present station-averaged results, a practice that is only valid if the anisotropic structure can be approximated by a single layer of anisotropy with a horizontal axis of symmetry (Silver & Savage, 1994). The third reason is that there is no estimate for the depth of the source of anisotropy, which limits viable interpretations of the SWS measurements. In the current study, we measure SWS measurements at an unprecedented number of stations in the EHS and surrounding areas, probe the presence of complex anisotropy by examining the azimuthal variation of individual splitting parameters, estimate the depth of anisotropy using the spatial coherency approach (Gao et al., 2010; Liu & Gao, 2011), and propose a geodynamic model involving slab subduction and rollback to explain the observed splitting parameters in the inadequately investigated but tectonically interesting area.

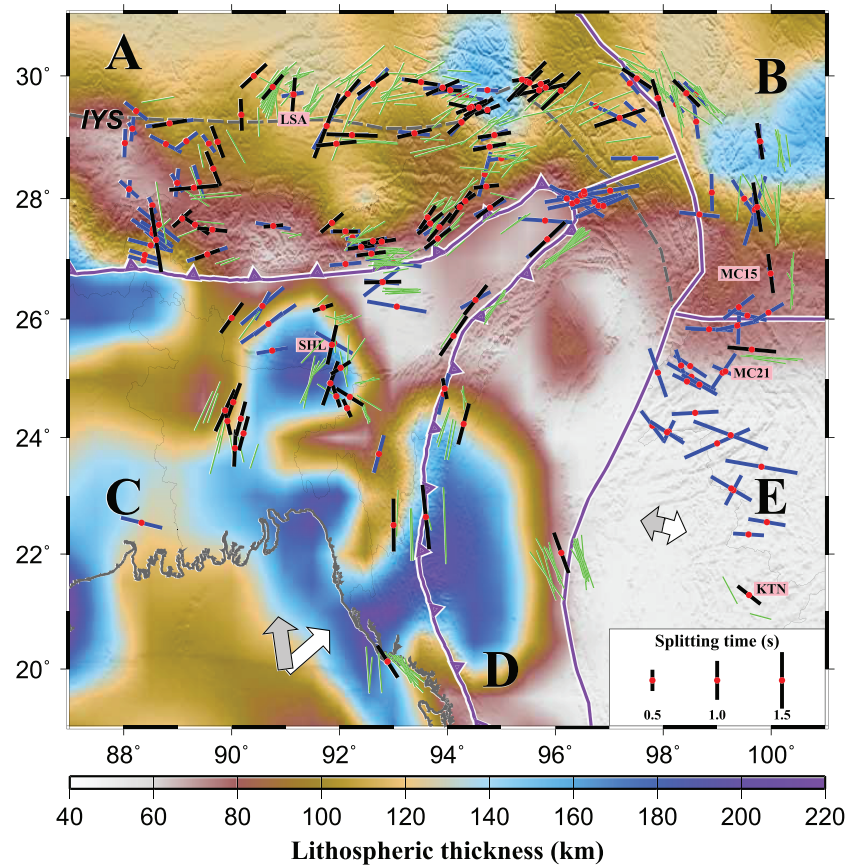


Figure 2. Shear wave splitting measurements from this (green and black bars) and previous (blue bars) studies. The thin green bars indicate individual measurements plotted above the 200-km ray-piercing points, while the thick black bars represent station-averaged ones plotted at the stations (red circles) obtained from this study. The blue bars are station-averaged results from previous studies. The purple lines are the boundaries among different subregions, most of which are consistent with the tectonic boundaries (Hazarika et al., 2013). The background image shows lithospheric thickness (Pasyanos et al., 2014), and labels A–E indicate subregions.

3. Data and Methods

The data processing parameters and procedure are identical to those described in Liu and Gao (2013) and are briefly summarized below. The broadband XKS data used in the study were recorded by a total of 115 three-component broadband seismic stations in the area between 88°E and 100°E, and 20°N and 30°N (Figures 1 and 2), over periods ranging from July 1991 to January 2018. Data from 70 stations were requested from the Incorporated Research Institutions for Seismology Data Management Center, and those from 45 stations were from the Indian National Geophysical Research Institute (Saikia et al., 2018). Among these stations, station LSA (longitude 91.13°, latitude 29.70°) on the Lhasa Terrane has recorded seismograms for over 20 years, and complex anisotropy has been revealed from a total of 67 SWS measurements at this station (Gao & Liu, 2009). The supporting information Figure S1a shows the distribution of the 130 teleseismic events that have provided at least one well-defined measurement used in this study.

The seismograms were band pass filtered in the frequency range of 0.04–0.5 Hz, and those with a signal-to-noise ratio that is smaller than 2.0 on the radial component were rejected by an automatic data selection routine. The SWS parameters were computed using the minimization of transverse energy approach of Silver and Chan (1991). After automatic calculation and ranking, we manually checked all the measurements, and if necessary, some of the data processing parameters were adjusted, including the beginning and ending time of the XKS window, band-pass filtering frequencies, and the ranking. In addition to well-defined splitting parameters, null measurements, which are characterized by strong XKS arrivals on the radial

component but nearly no XKS energy on the transverse component, are also identified. They indicate that the back-azimuth (BAZ) of the event is parallel or perpendicular to the fast orientation, or the mantle beneath the station, when integrated along the entire ray path from the core-mantle boundary to the surface, is an apparent isotropic medium (Silver & Chan, 1991).

4. Results

A total of 431 well-defined (Quality A or B) SWS measurements was obtained at 85 stations (including 364 observations at 84 stations from this study and 67 from station LSA obtained by Gao & Liu, 2009). Among them, 53 are PKS, 114 are SKKS, and 264 are SKS measurements (Figure S1). Besides the Quality A and B measurements, 632 null measurements were observed in the study area, including 30 (among totally 115) stations with all-null measurements (Figure S2). The individual and station-averaged measurements are shown in Figure 2, while the original and corrected radial and transverse components and other related data for each of the measurements can be found online (<http://web.mst.edu/~sgao/Hima-SWS>).

For the entire study area, the circular mean value of the fast orientations is $45.5^\circ \pm 47.6^\circ$, while the splitting times vary from 0.25 to 2.15 s with an average of 0.93 ± 0.32 s, which is comparable to the global average of 1.0 s for continents (Silver, 1996). In the following the study area is divided into five subregions according to the tectonic background and the spatial distribution of the splitting parameters, as shown in Figure 2.

4.1. Area A

Area A includes the Himalayan Orogenic Belt and the Lhasa Terrane of the Tibetan Plateau and contains 232 well-defined measurements from 53 stations. The fast orientations are characterized by a circular average of $57.8^\circ \pm 27.5^\circ$, while the corresponding splitting time has a mean value of 0.84 ± 0.30 s. The dominant fast orientation shows a systematic spatial variation, ranging from NE-SW in the eastern part to E-W in the central area and NW-SE at the southwestern corner of the area. Clear splitting was observed at most of the stations in this area, where many previous studies proposed that there is weak or no mantle anisotropy (Chen et al., 2010; Fu et al., 2008; Huang et al., 2000; Zhao et al., 2014). As demonstrated in Figure S2, the XKS events are concentrated in three narrow BAZ ranges: $\sim 120^\circ$ for SKS, $\sim 280^\circ$ for SKKS, and $\sim 20^\circ$ for PKS, which are largely parallel or orthogonal to the dominant fast orientations in this area (Figure S1), leading to numerous null measurements. In particular, the vast majority of the SKS events, which were used exclusively by most previous SWS studies in this area, are located in the southwest Pacific subduction zone and thus have a narrow BAZ range that is almost identical to the dominant fast or slow orientation in the area. The inclusion of the PKS and SKKS phases greatly increased the BAZ coverage and consequently revealed the existence of observable azimuthal anisotropy.

4.2. Area B

Area B is separated from Area A by the Nujiang suture and contains 59 Quality A or B measurements from six stations. The fast orientations in this area vary from NW-SE in the northern part to N-S in the southern part, with a circular mean of $152.8^\circ \pm 22.7^\circ$, which is consistent with the surface tectonic fabrics and GPS-measured crust movement direction relative to the stable interior of Eurasia (Gan et al., 2007). The mean splitting time is 1.00 ± 0.30 s. The pattern of spatial variation of the fast orientations is in agreement with the results of previous studies (Chang et al., 2015; Kong et al., 2018; Sol et al., 2007; Wang et al., 2008).

4.3. Area C

Area C is situated in the northeastern Indian plate. The fast orientations from the 102 measurements at 24 stations are mostly N-S with a mean value of $29.8^\circ \pm 43.4^\circ$, and the mean splitting time is 1.02 ± 0.31 s. The fast orientations, especially those at stations away from the northern and eastern boundaries of this area, are mostly N-S, which differ significantly from the dominantly NE-SW orientations observed at the rest of the Indian continent (Figure 1; see also Jolivet et al., 2018). In this area, there were limited splitting measurements observed in previous investigations (Figure 1), most of which concluded that the mantle is isotropic or weakly anisotropic on the basis of a limited number of null measurements (Barruol & Hoffmann, 1999; Chen & Özalaybey, 1998; Sandvol et al., 1997). In sharp contrast, results from this study show clear anisotropy beneath this area. A total of 164 null measurements from 25 stations was obtained from this study in Area C.

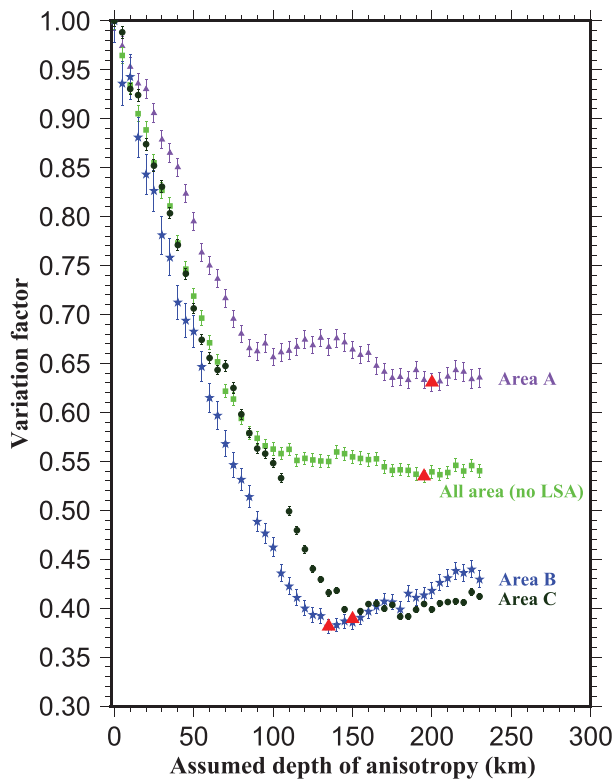


Figure 3. Spatial variation factors plotted against assumed depth of anisotropy for shear wave splitting measurements in areas A–C. The red triangles on the curves represent the minimum variation factors corresponding to the optimal depths of anisotropy.

the spatial coherency technique to estimate the depth of anisotropy for some of the five subregions. The description of the technique and the accompanying FORTRAN program can be found in Gao and Liu (2012) and are briefly summarized here. The spatial variation factor, which is the weighted sum of the circular standard deviation of the fast orientations and the arithmetic standard deviation of the splitting times in overlapping rectangle blocks, is calculated for each assumed depth from 0 to 400 km with an interval of 5 km. The optimal anisotropy depth corresponds to the minimum variation factor on the resulting curve. The resulting optimal depth of the anisotropic layer is 200, 135, and 160 km beneath areas A, B, and C, respectively (Figure 3). The estimated depth of anisotropy beneath Area A is greater than the lithospheric thickness of 80–160 km in the LITHO1.0 model (Figure 2; Pasyanos et al., 2014), suggesting that the observed seismic anisotropy mostly originates from the upper asthenosphere. In contrast, for Areas B and C, where the lithospheric thickness obtained from several seismic techniques (Kumar et al., 2013; Pasyanos et al., 2014) is comparable to the estimated depth of 135 and 160 km (Figure 2; Pasyanos et al., 2014), the observed anisotropy is most likely from the lithosphere-asthenosphere transitional zone (Debayle & Ricard, 2013), as proposed elsewhere such as the eastern United States (Yang et al., 2017). For Areas D and E, the distance between the stations is too large to apply the spatial coherency approach to estimate the depth of anisotropy.

In Area E, apparent azimuthal variations of the splitting measurements are observed at station KTN from events with different BAZs (Figures S3a and S3b), an observation that is consistent with a source that is deeper than the depth at which the corresponding Fresnel zones overlap (Alsina & Snieder, 1995). Under the assumption that the lithospheric thickness of 40–80 km (Figure 2) in this area is accurately determined, the source of anisotropy is located in the upper asthenosphere.

5.2. Contribution of Lithospheric Fabrics

Vertically coherent deformation of the crust and mantle can lead to seismic azimuthal anisotropy, with fast orientations being predominantly parallel to the strike of transpressional tectonics (Silver, 1996; Silver & Chan, 1991; Wang et al., 2008). Some previous SWS studies argue that vertically coherent lithospheric

4.4. Area D

Area D is part of the Indo-Burma range between the Indian plate and the Indochina block. Most of the measurements from this study are along the western and eastern boundaries of this region, which was not sampled by previous studies except for the NW corner (Figure 2). There are 34 measurements from four stations in this area. The splitting parameters are characterized by N-S fast orientations ($165.0^\circ \pm 13.1^\circ$), similar to those in the northeast part of the Indian plate, while the average splitting time of 1.17 ± 0.30 s is apparently greater than that of Area C. Stations along the western margin of this area and those along the eastern margin of Area C show a remarkable parallelism with the Arakan trench.

4.5. Area E

Area E is the westernmost part of the Indochina block. Its northern boundary separates the area with dominantly N-S fast orientations in Area B and E-W fast orientations in the northern part of Area E. The two closest stations in the two areas, MC15 in Area B and MC21 in Area E (Figure 2), have a distance of about 100 km. The splitting times of the two stations in this area have a mean value of 1.10 ± 0.42 s, which is comparable to that of the global average. At station KTN, the event from the south has a nearly E-W fast orientation, while that from the west shows a nearly N-S fast orientation (Figures 2, S3a, and S3b).

5. Discussion

5.1. Estimation of the Depth of Anisotropy

The dominantly simple anisotropy (except for station LSA, beneath which complex anisotropy has been identified by Gao & Liu, 2009) and densely spaced stations in the study area provide the necessary conditions to apply

deformation dominates the anisotropy in the SE Tibetan Plateau on the basis of the consistent directions between the GPS and fast orientations (Sol et al., 2007; Wang et al., 2008). However, several phenomena described below imply that lithospheric fabrics have an insignificant contribution to the observed azimuthal anisotropy in most of the study area.

First, some of the observed fast orientations are not consistent with the dominant strike of the major compressional tectonic belts. For example, in the westernmost and easternmost parts of Area A, most of the fast orientations are perpendicular to the strike of the Indus-Yalu suture (Figure 2). Second, there is no significant increase in the observed splitting times at the stations near the shear zones, where the shear strain is expected to be more localized (Figure S4). If the anisotropy is mostly produced by lithospheric compressional strain, larger splitting times are expected along the suture zones. Third, there is no positive correlation between the splitting times and lithospheric thickness, an observation that is contradicting with the mechanism that thicker lithosphere possesses larger splitting times under the assumption of a constant degree of anisotropy in the lithosphere. Finally, results of the anisotropy depth analysis (Figure 3) suggest that the observed anisotropy is primarily from the lithosphere-asthenosphere transition zone or the upper asthenosphere. Therefore, the observed azimuthal anisotropy is most likely located in the asthenosphere or its transitional layer with the lithosphere.

5.3. Mantle Flow-Induced Anisotropy

The controlling parameter to generate azimuthal anisotropy in subduction zone regions is the trench migration rate (Long & Silver, 2009). A 3-D flow model controlled by the rollback of the slab is proposed beneath subducting slabs (Long & Becker, 2010; Long & Wirth, 2013; Sternai et al., 2014).

5.3.1. APM-Related Asthenospheric Flow

It has long been recognized that in the asthenosphere, simple shear originating from the flow gradient caused by the relative movement between the lithosphere and asthenosphere could result in azimuthal anisotropy that is parallel to the direction of shear (Silver, 1996; Silver & Chan, 1991; Zhang & Karato, 1995). Assuming a stationary asthenosphere (or both the asthenosphere and the lithosphere move at the opposite direction or the same direction with different speed), APM can induce azimuthal anisotropy. In the no-net-rotation NNR-MORVEL56 model (Argus et al., 2011), the moving direction of the Indian plate portion of the study area (Area C) is about 50° clockwise from the north, at a speed of nearly 50 mm/year, while in the HS3-NUVEL-1A model (Gripp & Gordon, 2002) that employs a fixed hot spot reference frame, the area moves toward the north with a similar speed (Figure 2).

The fast orientations observed in most parts of the Indian continent are mostly NE-SW (Jolivet et al., 2018), which is consistent with the APM direction predicted based on fixed hot spot APM models (Gripp & Gordon, 2002). Although the dominantly NE-SW and N-S fast orientations observed in the NE corner of the Indian plate (Area C) are approximately parallel to the APM directions, the systematic spatial variations of the fast orientations and their correspondence with the trends of the northern and eastern margins of this region make it difficult to argue that APM plays a determinant role in producing the observed anisotropy in this area. Similarly, while a small portion of the observed fast orientations (e.g., the northern part of Area E and the central part of Area A) is consistent with the APM direction, the fact that the majority of the measurements in the same subregions are inconsistent with the APM direction places doubt on the role of APM in producing the observed azimuthal anisotropy.

5.3.2. Rollback and Slab Gap-Induced Mantle Flow: A Preliminary Model

The absence of significant lithospheric and APM-induced asthenospheric contributions to the observed anisotropy indicates that the observed anisotropy is dominated by localized mantle flow systems. One of the viable models is a toroidal flow driven by slab rollback (Figure 4). Under this model, the subsurface trench parallel flow might be responsible for the dominantly N-S fast orientations in Areas C and D. The controlling parameter to generate azimuthal anisotropy in subduction zone regions is the trench migration rate (Long & Silver, 2009). A 3-D flow model controlled by the rollback of the slab is proposed beneath subducting slabs elsewhere (Long & Becker, 2010; Long & Silver, 2009; Long & Wirth, 2013; Sternai et al., 2014). Most studies suggest that the eastward subduction of the Indian plate is undergoing westward trench rollback (Kundu & Gahalaut, 2012; Li et al., 2008; Rao & Kumar, 1999). The fact that the observed anisotropy in NE India (Area C) is parallel to the predicted subsurface flow direction rather than the APM direction may suggest that the latter is overprinted by the former. The rollback-induced westward corner flow in the mantle wedge may be

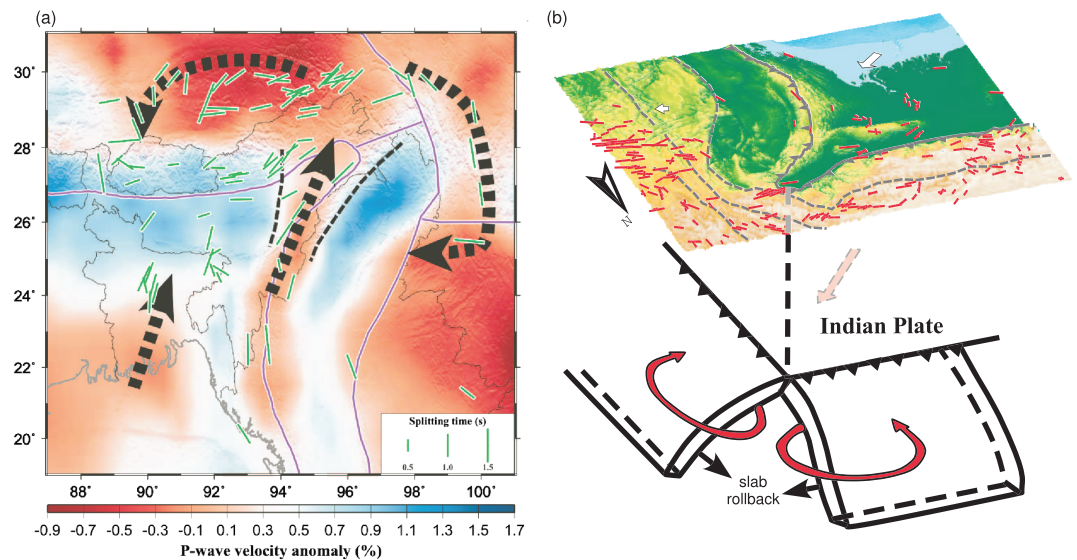


Figure 4. (a) Schematic diagram showing direction of flow lines in the asthenosphere relative to the lithosphere beneath the eastern Himalayan syntaxis and surrounding areas. The green bars represent station-averaged shear-wave splitting measurements. The background shows P -wave velocity anomaly at the depth of 200 km (Li et al., 2006). The thick dashed arrows show asthenosphere flow induced by the absolute plate motion and slab rollback, while the thin dashed lines represent the location of the slab gap. (b) A three-dimensional representation of the mantle flow model.

responsible for the mostly E-W fast orientations observed in Area E and the rest of northern Indochina Peninsula (Yu et al., 2018).

Our favored model (Figure 4) attributes the spatial variation of the observed anisotropy in Areas A and B to a toroidal flow system driven by the slab rollback and modulated by a slab gap between the northward and eastward subducting slabs. Seismic tomography and receiver function investigations have revealed the presence of the slab gap in the vicinity of the EHS at a depth of 200 km (Kumar et al., 2016; Li et al., 2006; Xu et al., 2018). We propose that the trench-parallel subslab flow escapes from the slab gap and migrates to the mantle wedge beneath Areas A and B, leading to the observed pattern of anisotropy (Figure 4). This model and the observed spatial distribution of azimuthal anisotropy are consistent with rollback-driven flow systems in the vicinity of slab gaps revealed in numerical modeling studies (Becker & Faccenna, 2009; Duarte et al., 2013; Schellart, 2004; Stegman et al., 2006).

6. Conclusions

Measurements of seismic azimuthal anisotropy using SWS in the vicinity of the EHS reveal systematic spatial variations of the splitting parameters. Spatial coherency analysis of the splitting parameters suggests that the source of anisotropy is mostly located in the upper asthenosphere or the transitional layer between the lithosphere and asthenosphere. The observed spatial pattern of anisotropy may be explained by a model involving three flow systems: a subslab trench-parallel flow and a trench-perpendicular flow in the mantle wedge driven by the rollback of the eastward subducting Indian plate and a toroidal flow system escaping from a slab gap into the mantle wedge of both the northward and eastward subducting Indian slabs.

References

- Alsina, D., & Snieder, R. (1995). Small-scale sublithospheric continental mantle deformation: Constraints from SKS splitting observations. *Geophysical Journal International*, 123(2), 431–448. <https://doi.org/10.1111/j.1365-246X.1995.tb06864.x>
- Argus, D. F., Gordon, R. G., & DeMets, C. (2011). Geologically current motion of 56 plates relative to the no-net-rotation reference frame. *Geochemistry, Geophysics, Geosystems*, 12, Q11001. <https://doi.org/10.1029/2011GC003751>
- Barruol, G., & Hoffmann, R. (1999). Upper mantle anisotropy beneath the Geoscope stations. *Journal of Geophysical Research*, 104(B5), 10,757–10,773. <https://doi.org/10.1029/1999JB900033>
- Becker, T. W., & Faccenna, C. (2009). A review of the role of subduction dynamics for regional and global plate motions. In *Subduction Zone Geodynamics*, (pp. 3–34). Berlin, Heidelberg: Springer.

Acknowledgments

All the data used in the study were obtained from the IRIS DMC (<http://ds.iris.edu/ds/nodes/dmc> [last accessed: January 2018]) and the data source from the Indian National Geophysical Research Institute described in Saikia et al. (2018); <http://www.facweb.iitkgp.ernet.in/~arunsingh> [last accessed: October 2018]. We thank Rob Porritt, Jeroen Ritsema, and an anonymous reviewer for constructive reviews. This study was partially supported by the China Scholarship Council and Ocean University of China to L. L., by the National Natural Science Foundation of China under award 41876036 to S. L., and by the U.S. National Science Foundation under awards 0911346 and 1830644 to K. L. and S. G.

- Bracciali, L., Parrish, R. R., Najman, Y., Smye, A., Carter, A., & Wijbrans, J. R. (2016). Plio-Pleistocene exhumation of the eastern Himalayan syntaxis and its domal 'pop-up'. *Earth-Science Reviews*, *160*, 350–385. <https://doi.org/10.1016/j.earscirev.2016.07.010>
- Chang, L., Flesch, L. M., Wang, C. Y., & Ding, Z. (2015). Vertical coherence of deformation in lithosphere in the eastern Himalayan syntaxis using GPS, Quaternary fault slip rates, and shear wave splitting data. *Geophysical Research Letters*, *42*, 5813–5819. <https://doi.org/10.1002/2015GL064568>
- Chen, W. P., Martin, M., Tseng, T. L., Nowack, R. L., Hung, S. H., & Huang, B. S. (2010). Shear-wave birefringence and current configuration of converging lithosphere under Tibet. *Earth and Planetary Science Letters*, *295*, 297–304. <https://doi.org/10.1016/j.epsl.2010.04.017>
- Chen, W. P., & Özalaybey, S. (1998). Correlation between seismic anisotropy and Bouguer gravity anomalies in Tibet and its implications for lithospheric structures. *Geophysical Journal International*, *135*(1), 93–101. <https://doi.org/10.1046/j.1365-246X.1998.00611.x>
- Dasgupta, S., Mukhopadhyay, M., Bhattacharya, A., & Jana, T. K. (2003). The geometry of the Burmese-Andaman subducting lithosphere. *Journal of Seismology*, *7*(2), 155–174. <https://doi.org/10.1023/A:1023520105384>
- Debayle, E., & Ricard, Y. (2013). Seismic observations of large-scale deformation at the bottom of fast-moving plates. *Earth and Planetary Science Letters*, *376*, 165–177. <https://doi.org/10.1016/j.epsl.2013.06.025>
- Duarte, J. C., Schellart, W. P., & Cruden, A. R. (2013). Three-dimensional dynamic laboratory models of subduction with an overriding plate and variable interplate rheology. *Geophysical Journal International*, *195*(1), 47–66. <https://doi.org/10.1093/gji/ggt257>
- Flesch, L. M., Holt, W. E., Silver, P. G., Stephenson, M., Wang, C. Y., & Chan, W. W. (2005). Constraining the extent of crust-mantle coupling in central Asia using GPS, geologic, and shear wave splitting data. *Earth and Planetary Science Letters*, *238*(1–2), 248–268. <https://doi.org/10.1016/j.epsl.2005.06.023>
- Fu, Y. V., Chen, Y. J., Li, A., Zhou, S., Liang, X., Ye, G., et al. (2008). Indian mantle corner flow at southern Tibet revealed by shear wave splitting measurements. *Geophysical Research Letters*, *35*, L02308. <https://doi.org/10.1029/2007GL031753>
- Gan, W., Zhang, P., Shen, Z., Niu, Z., Wang, M., Wan, Y., et al. (2007). Present-day crustal motion within the Tibetan Plateau inferred from GPS measurements. *Journal of Geophysical Research*, *112*, B08416. <https://doi.org/10.1029/2005JB004120>
- Gao, S., Davis, P. M., Liu, H., Slack, P. D., Zorin, Y. A., Mordvinova, V. V., et al. (1994). Seismic anisotropy and mantle flow beneath the Baikal rift zone. *Nature*, *371*(6493), 149. <https://doi.org/10.1038/371149a0>
- Gao, S. S., & Liu, K. H. (2009). Significant seismic anisotropy beneath the southern Lhasa Terrane, Tibetan Plateau. *Geochemistry, Geophysics, Geosystems*, *10*, Q02008. <https://doi.org/10.1029/2008GC002227>
- Gao, S. S., & Liu, K. H. (2012). AnisDep: A FORTRAN program for the estimation of the depth of anisotropy using spatial coherency of shear-wave splitting parameters. *Computers & Geosciences*, *49*, 330–333. <https://doi.org/10.1016/j.cageo.2012.01.020>
- Gao, S. S., Liu, K. H., & Abdelsalam, M. G. (2010). Seismic anisotropy beneath the Afar Depression and adjacent areas: Implications for mantle flow. *Journal of Geophysical Research*, *115*, B12330. <https://doi.org/10.1029/2009JB007141>
- Giacomuzzi, G., Civalleri, M., de Gori, P., & Chiarabba, C. (2012). A 3D Vs model of the upper mantle beneath Italy: Insight on the geodynamics of central Mediterranean. *Earth and Planetary Science Letters*, *335*, 105–120. <https://doi.org/10.1016/j.epsl.2012.05.004>
- Gripp, A. E., & Gordon, R. G. (2002). Young tracks of hotspots and current plate velocities. *Geophysical Journal International*, *150*(2), 321–361. <https://doi.org/10.1046/j.1365-246X.2002.01627.x>
- Hazarika, D., Yadav, D. K., Sriram, V., & Rai, A. (2013). Upper mantle anisotropy beneath northeast India-Asia collision zone from shear-wave splitting analysis. *International Journal of Earth Sciences*, *102*(7), 2061–2076. <https://doi.org/10.1007/s00531-013-0922-4>
- Heintz, M., Kumar, V. P., Gaur, V. K., Priestley, K., Rai, S. S., & Prakasam, K. S. (2009). Anisotropy of the Indian continental lithospheric mantle. *Geophysical Journal International*, *179*(3), 1341–1360. <https://doi.org/10.1111/j.1365-246X.2009.04395.x>
- Huang, J., & Zhao, D. (2006). High-resolution mantle tomography of China and surrounding regions. *Journal of Geophysical Research*, *111*, B09305. <https://doi.org/10.1029/2005JB004066>
- Huang, W. C., Ni, J. F., Tilmann, F., Nelson, D., Guo, J., Zhao, W., et al. (2000). Seismic polarization anisotropy beneath the central Tibetan Plateau. *Journal of Geophysical Research*, *105*(B12), 27,979–27,989. <https://doi.org/10.1029/2000JB900339>
- Huang, Z., Wang, L., Xu, M., Ding, Z., Wu, Y., Wang, P., et al. (2015). Teleseismic shear-wave splitting in SE Tibet: Insight into complex crust and upper-mantle deformation. *Earth and Planetary Science Letters*, *432*, 354–362. <https://doi.org/10.1016/j.epsl.2015.10.027>
- Huang, Z., Wang, P., Xu, M., Wang, L., Ding, Z., Wu, Y., et al. (2015). Mantle structure and dynamics beneath SE Tibet revealed by new seismic images. *Earth and Planetary Science Letters*, *411*, 100–111. <https://doi.org/10.1016/j.epsl.2014.11.040>
- Huang, Z., Zhao, D., & Wang, L. (2015). P wave tomography and anisotropy beneath Southeast Asia: Insight into mantle dynamics. *Journal of Geophysical Research: Solid Earth*, *120*, 5154–5174. <https://doi.org/10.1002/2015JB012098>
- Jadamec, M. A., & Billen, M. I. (2010). Reconciling surface plate motions with rapid three-dimensional mantle flow around a slab edge. *Nature*, *465*(7296), 338. <https://doi.org/10.1038/nature09053>
- Jadamec, M. A., & Billen, M. I. (2012). The role of rheology and slab shape on rapid mantle flow: Three-dimensional numerical models of the Alaska slab edge. *Journal of Geophysical Research*, *117*, B02304. <https://doi.org/10.1029/2011JB008563>
- Jolivet, L., Faccenna, C., Becker, T., Tesauero, M., Sternai, P., & Bouilhol, P. (2018). Mantle flow and deforming continents: From India-Asia convergence to Pacific subduction. *Tectonics*, *37*, 2887–2914. <https://doi.org/10.1029/2018TC005036>
- Katayama, I., & Karato, S. I. (2006). Effect of temperature on the B-to C-type olivine fabric transition and implication for flow pattern in subduction zones. *Physics of the Earth and Planetary Interiors*, *157*(1–2), 33–45. <https://doi.org/10.1016/j.pepi.2006.03.005>
- Kong, F., Wu, J., Liu, L., Liu, K. H., Song, J., Li, J., & Gao, S. S. (2018). Azimuthal anisotropy and mantle flow underneath the southeastern Tibetan Plateau and northern Indochina Peninsula revealed by shear wave splitting analyses. *Tectonophysics*, *747*, 68–78. <https://doi.org/10.1016/j.tecto.2018.09.013>
- Kumar, P., Ravi Kumar, M., Sriyayanthi, G., Arora, K., Srinagesh, D., Chadha, R. K., & Sen, M. K. (2013). Imaging the lithosphere-asthenosphere boundary of the Indian plate using converted wave techniques. *Journal of Geophysical Research: Solid Earth*, *118*, 5307–5319. <https://doi.org/10.1002/jgrb.50366>
- Kumar, P., Sriyayanthi, G., & Ravi Kumar, M. (2016). Seismic evidence for tearing in the subducting Indian slab beneath the Andaman arc. *Geophysical Research Letters*, *43*, 4899–4904. <https://doi.org/10.1002/2016GL068590>
- Kundu, B., & Gahalaut, V. K. (2012). Earthquake occurrence processes in the Indo-Burmese wedge and Sagaing fault region. *Tectonophysics*, *524*, 135–146. <https://doi.org/10.1016/j.tecto.2011.12.031>
- Lei, J., & Zhao, D. (2016). Teleseismic P-wave tomography and mantle dynamics beneath Eastern Tibet. *Geochemistry, Geophysics, Geosystems*, *17*, 1861–1884. <https://doi.org/10.1002/2016GC006262>
- Lei, J., Zhao, D., & Su, Y. (2009). Insight into the origin of the Tengchong intraplate volcano and seismotectonics in southwest China from local and teleseismic data. *Journal of Geophysical Research*, *114*, B05302. <https://doi.org/10.1029/2008JB005881>

- Lev, E., Long, M. D., & van der Hilst, R. D. (2006). Seismic anisotropy in Eastern Tibet from shear wave splitting reveals changes in lithospheric deformation. *Earth and Planetary Science Letters*, 251(3-4), 293–304. <https://doi.org/10.1016/j.epsl.2006.09.018>
- Li, C., van der Hilst, R. D., Meltzer, A. S., & Engdahl, E. R. (2008). Subduction of the Indian lithosphere beneath the Tibetan Plateau and Burma. *Earth and Planetary Science Letters*, 274(1-2), 157–168. <https://doi.org/10.1016/j.epsl.2008.07.016>
- Li, C., van der Hilst, R. D., & Toksöz, M. N. (2006). Constraining *P*-wave velocity variation in the upper mantle beneath southeast Asia. *Physics of the Earth and Planetary Interiors*, 154, 180–195. <https://doi.org/10.1016/j.pepi.2005.09.008>
- Li, Y., Wu, Q., Pan, J., Zhang, F., & Yu, D. (2013). An upper-mantle *S*-wave velocity model for East Asia from Rayleigh wave tomography. *Earth and Planetary Science Letters*, 377, 367–377. <https://doi.org/10.1016/j.epsl.2013.06.033>
- Liu, K. H., & Gao, S. S. (2011). Estimation of the depth of anisotropy using spatial coherency of shear-wave splitting parameters. *Bulletin of the Seismological Society of America*, 101, 2153–2161. <https://doi.org/10.1785/0120100258>
- Liu, K. H., & Gao, S. S. (2013). Making reliable shear-wave splitting measurements. *Bulletin of the Seismological Society of America*, 103(5), 2680–2693. <https://doi.org/10.1785/0120120355>
- Long, M. D., & Becker, T. W. (2010). Mantle dynamics and seismic anisotropy. *Earth and Planetary Science Letters*, 297(3-4), 341–354. <https://doi.org/10.1016/j.epsl.2010.06.036>
- Long, M. D., & Silver, P. G. (2008). The subduction zone flow field from seismic anisotropy: A global view. *Science*, 319(5861), 315–318. <https://doi.org/10.1126/science.1150809>
- Long, M. D., & Silver, P. G. (2009). Shear wave splitting anisotropy: Measurements, interpretation, and new directions. *Surveys in Geophysics*, 30, 407–461. <https://doi.org/10.1007/s10712-009-9075-1>
- Long, M. D., & Wirth, E. A. (2013). Mantle flow in subduction systems: The mantle wedge flow field and implications for wedge processes. *Journal of Geophysical Research: Solid Earth*, 118, 583–606. <https://doi.org/10.1002/jgrb.50063>
- Lucente, F. P., Chiarabba, C., Cimini, G. B., & Giardini, D. (1999). Tomographic constraints on the geodynamic evolution of the Italian region. *Journal of Geophysical Research*, 104(B9), 20,307–20,327. <https://doi.org/10.1029/1999JB900147>
- Ni, J. F., Guzman-Speziale, M., Bevis, M., Holt, W. E., Wallace, T. C., & Seager, W. R. (1989). Accretionary tectonics of Burma and the three-dimensional geometry of the Burma subduction zone. *Geology*, 17(1), 68–71. [https://doi.org/10.1130/00917613\(1989\)017<0068:ATOBAT>2.3.CO;2](https://doi.org/10.1130/00917613(1989)017<0068:ATOBAT>2.3.CO;2)
- Pasyanos, M. E., Masters, T. G., Laske, G., & Ma, Z. (2014). LITHO1.0: An updated crust and lithospheric model of the Earth. *Journal of Geophysical Research: Solid Earth*, 119, 2153–2173. <https://doi.org/10.1002/2013JB010626>
- Powell, C. M., & Conaghan, P. J. (1973). Plate tectonics and the Himalayas. *Earth and Planetary Science Letters*, 20(1), 1–12. [https://doi.org/10.1016/0012-821X\(73\)90134-9](https://doi.org/10.1016/0012-821X(73)90134-9)
- Rao, N. P., & Kumar, M. R. (1999). Evidences for cessation of Indian plate subduction in the Burmese arc region. *Geophysical Research Letters*, 26(20), 3149–3152. <https://doi.org/10.1029/1999GL005396>
- Reyners, M., Gledhill, K., & Waters, D. (1991). Tearing of the subducted Australian plate during the Te Anau, New Zealand, earthquake of 1988 June 3. *Geophysical Journal International*, 104(1), 105–115. <https://doi.org/10.1111/j.1365-246X.1991.tb02497.x>
- Roy, S. K., Srinagesh, D., Saikia, D., Singh, A., & Kumar, M. R. (2012). Seismic anisotropy beneath the eastern Dharwar craton. *Lithosphere*, 4(4), 259–268. <https://doi.org/10.1130/L198.1>
- Saikia, D., Kumar, M. R., Singh, A., Roy, S. K., Raju, P. S., & Lyngdoh, A. C. (2018). Mantle deformation in the Eastern Himalaya, Burmese arc and adjoining regions. *Geochemistry, Geophysics, Geosystems*, 19, 4420–4432. <https://doi.org/10.1029/2018GC007691>
- Saikia, D., Ravi Kumar, M., Singh, A., Mohan, G., & Dattatrayam, R. S. (2010). Seismic anisotropy beneath the Indian continent from splitting of direct *S* waves. *Journal of Geophysical Research*, 115, B12315. <https://doi.org/10.1029/2009JB007009>
- Sandvol, E., Ni, J., Kind, R., & Zhao, W. (1997). Seismic anisotropy beneath the southern Himalayas-Tibet collision zone. *Journal of Geophysical Research*, 102(B8), 17,813–17,823. <https://doi.org/10.1029/97JB01424>
- Savage, M. K. (1999). Seismic anisotropy and mantle deformation: What have we learned from shear wave splitting? *Reviews of Geophysics*, 37(1), 65–106. <https://doi.org/10.1029/98RG02075>
- Schellart, W. P. (2004). Kinematics of subduction and subduction-induced flow in the upper mantle. *Journal of Geophysical Research*, 109, B07401. <https://doi.org/10.1029/2004JB002970>
- Silver, P. G. (1996). Seismic anisotropy beneath the continents: Probing the depths of geology. *Annual Review of Earth and Planetary Sciences*, 24, 385–432. <https://doi.org/10.1146/annurev.earth.24.1.385>
- Silver, P. G., & Chan, W. W. (1991). Shear wave splitting and subcontinental mantle deformation. *Journal of Geophysical Research*, 96(B10), 16,429–16,454. <https://doi.org/10.1029/91JB00899>
- Silver, P. G., & Savage, M. K. (1994). The interpretation of shear-wave splitting parameters in the presence of two anisotropic layers. *Geophysical Journal International*, 119(3), 949–963. <https://doi.org/10.1111/j.1365-246X.1994.tb04027.x>
- Singh, A., Kumar, M. R., & Raju, P. S. (2007). Mantle deformation in Sikkim and adjoining Himalaya: Evidences for a complex flow pattern. *Physics of the Earth and Planetary Interiors*, 164(3-4), 232–241. <https://doi.org/10.1016/j.pepi.2007.07.003>
- Singh, A., Kumar, M. R., Raju, P. S., & Ramesh, D. S. (2006). Shear wave anisotropy of the northeast Indian lithosphere. *Geophysical Research Letters*, 33, L16302. <https://doi.org/10.1029/2006GL026106>
- Socquet, A., Vigny, C., Chamot-Rooke, N., Simons, W., Rangin, C., & Ambrosius, B. (2006). India and Sunda plates motion and deformation along their boundary in Myanmar determined by GPS. *Journal of Geophysical Research*, 111, B05406. <https://doi.org/10.1029/2005JB003877>
- Sol, S., Meltzer, A., Burgmann, R., van der Hilst, R. D., King, R., Chen, Z., et al. (2007). Geodynamics of the southeastern Tibetan Plateau from seismic anisotropy and geodesy. *Geology*, 35(6), 563–566. <https://doi.org/10.1130/G23408A.1>
- Steckler, M. S., Mondal, D. R., Akhter, S. H., Seeber, L., Feng, L., Gale, J., et al. (2016). Locked and loading megathrust linked to active subduction beneath the Indo-Burman Ranges. *Nature Geoscience*, 9(8), 615. <https://doi.org/10.1038/ngeo2760>
- Stegman, D. R., Freeman, J., Schellart, W. P., Moresi, L., & May, D. (2006). Influence of trench width on subduction hinge retreat rates in 3-D models of slab rollback. *Geochemistry, Geophysics, Geosystems*, 7, Q03012. <https://doi.org/10.1029/2005GC001056>
- Sternai, P., Jolivet, L., Menant, A., & Gerya, T. (2014). Driving the upper plate surface deformation by slab rollback and mantle flow. *Earth and Planetary Science Letters*, 405, 110–118. <https://doi.org/10.1016/j.epsl.2014.08.023>
- Tapponnier, P., Peltzer, G. L. D. A. Y., le Dain, A. Y., Armijo, R., & Cobbold, P. (1982). Propagating extrusion tectonics in Asia: New insights from simple experiments with plasticine. *Geology*, 10(12), 611–616. [https://doi.org/10.1130/0091-7613\(1982\)10<611:PETIAN>2.0.CO;2](https://doi.org/10.1130/0091-7613(1982)10<611:PETIAN>2.0.CO;2)
- Wang, C. Y., Flesch, L. M., Silver, P. G., Chang, L. J., & Chan, W. W. (2008). Evidence for mechanically coupled lithosphere in central Asia and resulting implications. *Geology*, 36(5), 363–366. <https://doi.org/10.1130/G24450A.1>

- Xu, M., Huang, H., Huang, Z., Wang, P., Wang, L., Xu, M., et al. (2018). Insight into the subducted Indian slab and origin of the Tengchong volcano in SE Tibet from receiver function analysis. *Earth and Planetary Science Letters*, *482*, 567–579. <https://doi.org/10.1016/j.epsl.2017.11.048>
- Yang, B. B., Liu, Y., Dahm, H., Liu, K. H., & Gao, S. S. (2017). Seismic azimuthal anisotropy beneath the eastern United States and its geodynamic implications. *Geophysical Research Letters*, *44*, 2670–2678. <https://doi.org/10.1002/2016GL071227>
- Yin, A., & Harrison, T. M. (2000). Geologic evolution of the Himalayan-Tibetan orogen. *Annual Review of Earth and Planetary Sciences*, *28*(1), 211–280. <https://doi.org/10.1146/annurev.earth.28.1.211>
- Yu, Y., Gao, S. S., Liu, K. H., Yang, T., Xue, M., Le, K. P., & Gao, J. (2018). Characteristics of the mantle flow system beneath the Indochina Peninsula revealed by teleseismic shear wave splitting analysis. *Geochemistry, Geophysics, Geosystems*, *19*, 1519–1532. <https://doi.org/10.1002/2018GC007474>
- Zhang, J., Ji, J., Zhong, D., Ding, L., & He, S. (2004). Structural pattern of eastern Himalayan syntaxis in Namjagbarwa and its formation process. *Science in China Series D: Earth Sciences*, *47*(2), 138. <https://doi.org/10.1360/02yd0042>
- Zhang, S., & Karato, S. I. (1995). Lattice preferred orientation of olivine aggregates deformed in simple shear. *Nature*, *375*, 774–777. <https://doi.org/10.1038/375774a0>
- Zhao, J., Murodov, D., Huang, Y., Sun, Y., Pei, S., Liu, H., et al. (2014). Upper mantle deformation beneath central-southern Tibet revealed by shear wave splitting measurements. *Tectonophysics*, *627*, 135–140. <https://doi.org/10.1016/j.tecto.2013.11.003>